Composites: Part A 97 (2017) 51–59

Contents lists available at ScienceDirect

Composites: Part A

journal homepage: www.elsevier.com/locate/compositesa

Characterization of 3D fabric permeability with skew terms

Minyoung Yun [a], Hatice Sas [b], Pavel Simacek [a], Suresh G. Advani [a,*]

[a] Department of Mechanical Engineering and Center for Composite Materials, University of Delaware, Newark, DE 19716, United States
[b] Current affiliation: Department of Mechanical Engineering, Abdullah Gul University, Kayseri 38080, Turkey

ARTICLE INFO

Article history:
Received 27 September 2016
Received in revised form 13 December 2016
Accepted 15 December 2016
Available online 4 January 2017

Keywords:
A. Preform
B. Permeability
E. Liquid composite molding
E. Resin flow

ABSTRACT

Flow simulations can predict resin flow behavior and void formation locations in a preform. One important parameter for simulation is the preform permeability. For thick parts with distribution media on the surface, resin flow is three dimensional and through the thickness permeability is required for simulation. If the fabric is a 3D preform or unbalanced, the through the thickness (*Kzz*) and two skew components (*Kxz* and *Kyz*) must be characterized. The skew terms influence the flow behavior and hence the void formation. In this study, we present a measurement station that provides all six independent components of the permeability tensor from one experiment. The methodology uses the location data of the flow front with time and then couples it to an optimization algorithm and our flow simulation tool, LIMS (Liquid Injection Molding Simulation). The process is automated and experimental results are superimposed on the simulation results to confirm fidelity of the values determined.

1. Introduction

In the Liquid Composite Molding (LCM) process, a fiber preform is placed in a closed mold and a liquid resin is injected to fill all the empty spaces between the fibers. After the resin cures, the part is demolded. It is essential to understand the flow of resin through fiber preforms to manufacture a void free composite structure, hence the need to model the resin flow. Flow of resin in the fiber preform can be modeled as flow through anisotropic porous media in which Darcy's law describes the liquid flow through a reinforcement as:

$$\langle \boldsymbol{u} \rangle = \frac{\boldsymbol{K}}{\mu} \cdot \nabla p \tag{1}$$

Here $\langle \boldsymbol{u} \rangle$ is volume averaged velocity vector, μ is the viscosity, ∇p is the resin pressure gradient which drives the flow, and $\boldsymbol{K}$ is the permeability tensor that characterizes the mobility of the resin flow in various directions through the porous medium. Permeability is a second order symmetric tensor with six independent components. It is a material property that describes fiber resistance to the flow of liquid.

$$\boldsymbol{K} = \begin{bmatrix} K_{xx} & K_{xy} & K_{xz} \\ K_{xy} & K_{yy} & K_{yz} \\ K_{xz} & K_{yz} & K_{zz} \end{bmatrix} \tag{2}$$

Permeability tensor is an important input parameter in the simulation to describe the flow behavior of the resin during mold filling. For this reason, many studies on characterizing the permeability of a reinforcement fabric have been carried out [1–12]. In-plane principle permeability values were measured experimentally in 16 different methods in the study by Arbter et al. [5]. Han et al. developed a new method to measure in-plane principle permeability components of fiber preforms with high volume fraction using pressure transducers [12]. Okonkwo et al. [1] developed a methodology to obtain four permeability values (all in-plane permeability components and through thickness permeability) from a single experiment. In-plane and through thickness permeability were studied in depth by the researchers, however, the skew terms (K_{xz} and K_{yz}) for thick parts have not been addressed. Hatice et al. [11] are the first ones to consider the effect of through thickness skew term on the flow front. Through thickness skew term if present can affect the resin flow dynamics in LCM process to a significant degree as shown by examples simulated in Figs. 1 and 2. In Fig. 1, the resin flow advancement along the top is shown when the resin is injected into the preform. The injection gate is located at the center of a rectangular mold from the bottom side. One can easily see the effects of transverse skew terms on the movement of the impregnating resin along the top surface as compared to the bottom surface. The flow front center on the top surface shifts in the x direction in relation to the injection gate with the presence of non-zero K_{xz} skew term and in the y direction with the non-zero K_{yz} skew term. Fig. 2

* Corresponding author.
E-mail address: advani@udel.edu (S.G. Advani).

http://dx.doi.org/10.1016/j.compositesa.2016.12.030
1359-835X/

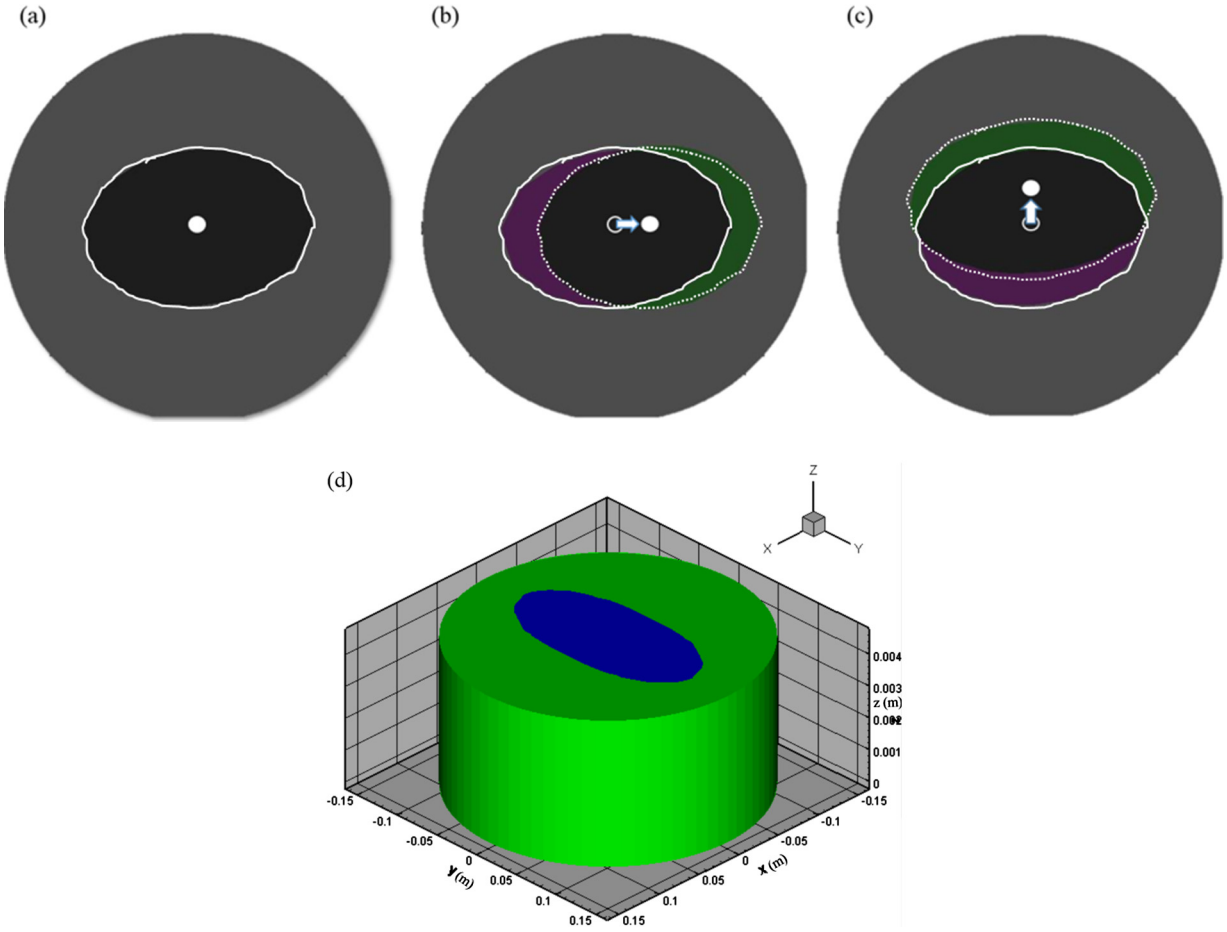

Fig. 1. (a) to (c) Flow front profiles on the top surface with a radial injection from the bottom surface of a mold at 120 s. (d) 3D geometry of the mesh used for the simulation study. Pink represents ellipse without skew terms. Green represents shifted ellipse due to skew terms. Black in (b) and (c) represent bottom and top surface overlapped areas. Solid line represents original ellipse. Dotted line represents shifted ellipse. (a) K_{xz}, $K_{yz} = 0$ (b) $K_{xz} = 5e{-}12\ m^2$, $K_{yz} = 0$ (c) $K_{xz} = 0$, $K_{yz} = 5e{-}12\ m^2$. For all simulations: $K_{xx} = 2e{-}10\ m^2$, $K_{yy} = 1e{-}10\ m^2$, $K_{zz} = 1e{-}12\ m^2$, $K_{xy} = 1e{-}11\ m^2$. (For interpretation of the references to color in this figure legend, the reader is referred to the web version of this article.)

shows the effects of transverse skew terms on resin flow patterns during impregnation into a complex 3D geometry. Resin of which viscosity is 0.1 Pa s is introduced from the center line gate which is located on the top side. Colors in the figure signify the arrival time of the resin at that location. Blue represents early times and red is later times. In Fig. 2(a), the flow fronts advance from the line gate reaching the edge of the trailer evenly at the same time along the top and the bottom. When through thickness skew terms are introduced in the simulation in Fig. 2(b), the flow fronts along the top and the bottom show substantial difference in the filling pattern which could lead to voids if the resin arrives at the vent before the preform is completely saturated.

Thick 3D preforms due to the complex weaving pattern exhibits asymmetric flow in the thickness direction which can be predicted if the skew terms from a permeability characterization experiment are provided as an input to the flow simulation. Hence, skew terms along with in-plane and transverse permeability of a preform should all be characterized to better understand resin flow behavior in LCM processes. In this paper, we present an optimized algorithm coupled with a permeability measurement station to obtain all six independent permeability components of the second order permeability tensor from a single experiment.

2. Approach

2.1. Methodology

Fig. 3 describes the methodology used to characterize the permeability tensor of the fabric from a single experiment. The methodology consists of two steps. The first step involves conducting a 3D flow experiment with a central injection gate on the bottom surface in a transparent mold. The movement of the flow front of the resin on the top and bottom side is recorded with two digital cameras. The images captured by digital cameras from the experiment are automatically processed to obtain resin flow front information at various times and to estimate initial set of three in-plane permeability components (K_{xx}, K_{yy}, K_{xy}). Initial through thickness permeability components (K_{zz}, K_{zx}, K_{zy}) are calculated using the grid method and image processing information. The second step uses this initial set of six permeability values as an input to LIMS (Liquid Injection Molding Simulation) to describe the flow behavior of the resin in a 3D mold. LIMS is a finite element/control volume based program that uses Darcy's law to predict the flow pattern within a porous preform as a function of time. Other input values in addition to the six components of the permeability tensor for the flow simulation are viscosity, inlet pressure or flow rate, and the fiber volume fraction. LIMS numerically simulates the flow of resin with the same geometry

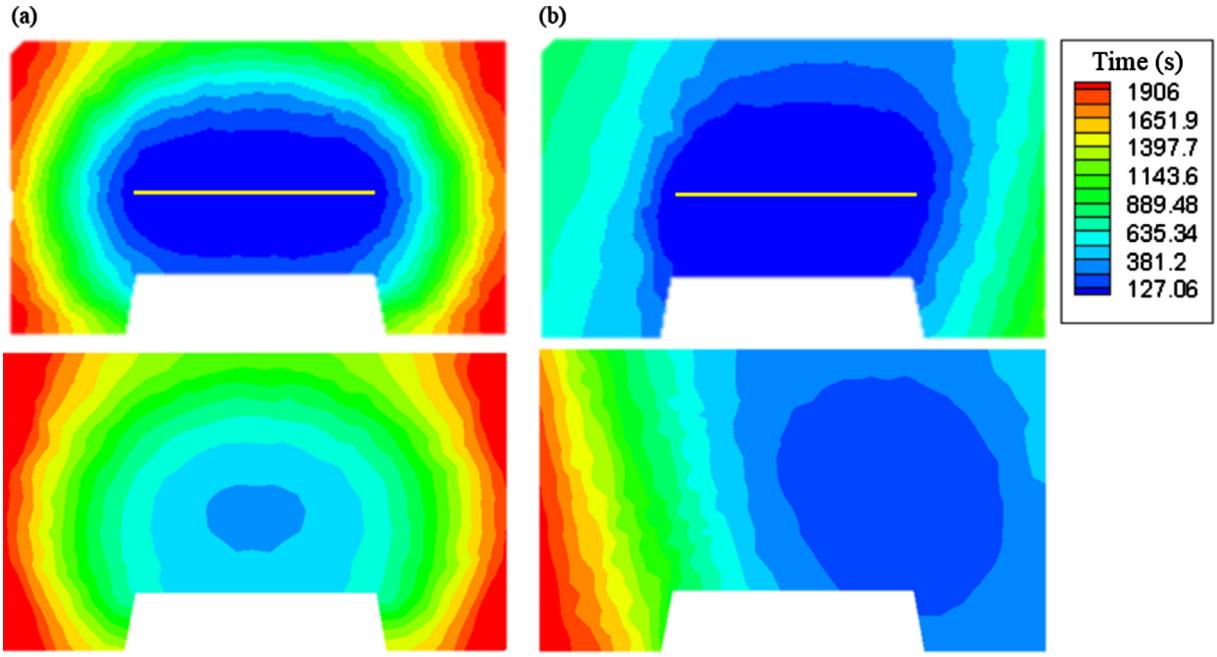

Fig. 2. Flow front profiles along the top (upper picture) and bottom (lower picture) surfaces of a 3D geometry from a line injection in the center along the X-axis on the top surface. (a) K_{xz}, K_{yz} = 0 (b) K_{xz} = 7e−12 m^2 K_{yz} = 7e−12 m^2 For both simulations: K_{xx} = 1e−10 m^2, K_{yy} = 1e−10 m^2, K_{zz} = 1e−12 m^2, K_{xy} = 0. (For interpretation of the references to color in this figure legend, the reader is referred to the web version of this article.)

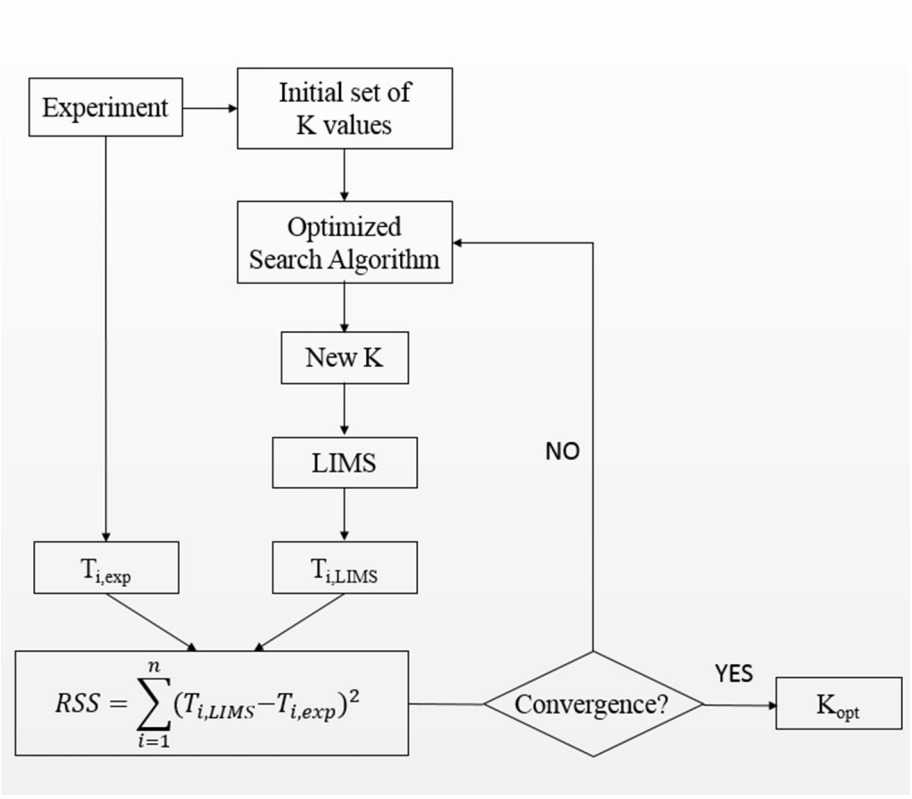

Fig. 3. Methodology for characterization of all six independent components of the permeability tensor from a single experiment.

and the inlet location as the experimental case. The flow front arrival times from the LIMS simulation are compared with the experimentally recorded flow fronts and the Residual Sum of Squares (RSS) is calculated. 7–8 flow fronts from each bottom and top are used for the RSS calculation. For the calculation, only the nodes that lie on the ellipses fitting the flow fronts and interpolated ones are considered which amounts to a total of 100–200 nodes.

$$RSS = \sum_{i=1}^{N} ((T_{i,exp} - T_{i,lims})^2) \quad (3)$$

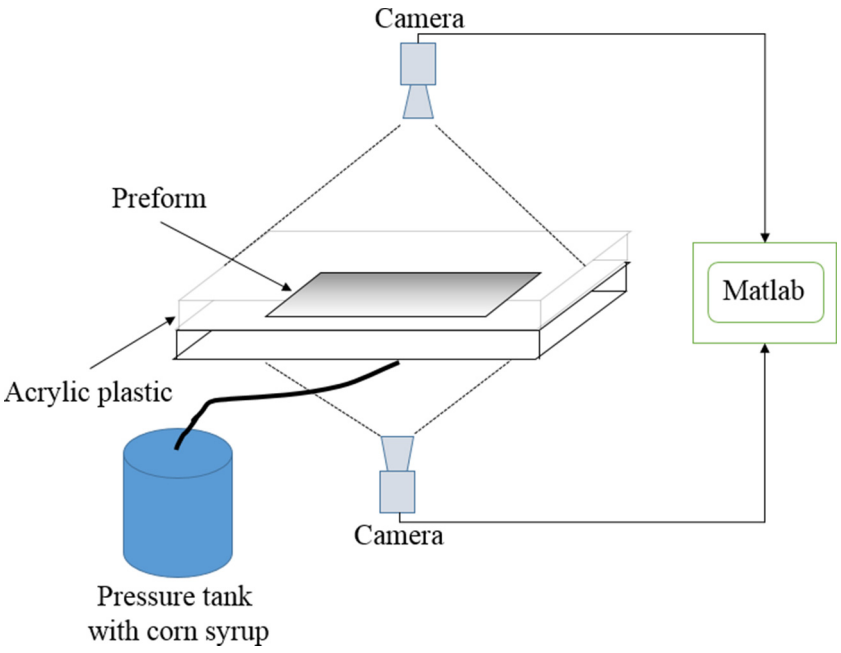

Fig. 4. Schematic of the experimental set up to characterize six independent components of the permeability tensor of a fiber preform from one experiment. (For interpretation of the references to color in this figure legend, the reader is referred to the web version of this article.)

where, N is the number of nodes filled with resin, $T_{i,exp}$ is a resin arrival time at each node during the experiment, and $T_{i,lims}$ is the arrival time calculated using LIMS. The permeability values in the LIMS simulation are systematically updated using the simplex optimization search algorithm. The coupled system of LIMS and the simplex search algorithm work in tandem to minimize the RSS. When the relative error between the fill times from the numerical simulation and experiments is less than 5%, the permeability set is deemed to be found and the search is ended.

The next two sections describe the experimental and the search algorithms in detail.

2.2. Experimental

Fig. 4 is a schematic describing the experimental setting. E glass woven fabric was used for the flow test as a reinforcement. First, fabrics are weighed to calculate the volume fraction and resin viscosity is measured. The fabric reinforcement is placed between two transparent acrylic molds with a spacer plate in between creating a picture frame mold as in a Resin Transfer Molding setting (RTM). The flat acrylic mold is 35 cm in width and length. The thickness of the mold plates is 5 cm. The fabric is compressed and clamped until the top and the bottom surface of the mold are flush with the spacer plate. The resin from a pressurized tank under constant pressure is injected through the center gate in the bottom mold. Test fluid (corn syrup) is used here because it is as viscous as a resin and easy to clean after the experiment is completed. Also, as the interest of the study is to investigate the flow behavior of resin, the use of corn syrup is valid and well known way to simulate resin flow. The resin flow is recorded through the transparent acrylic mold by two cameras mounted over the surfaces during the impregnation of resin into the fabric as shown in Fig. 4. Fluid pressure was measured with the pressure gauge at the pressure vessel.

Once the images are obtained from the experiment, they are analyzed to calculate initial in-plane permeability components as explained in the next section of the image processing step.

2.3. Image processing

After the experiment is recorded, the flow fronts in the images as seen from the top and the bottom surface at various times are fitted with ellipses with a least-squares fit method using MATLAB. This allows one to obtain the resin arrival time at any location. The accuracy of the methodology is confirmed by comparing the nodal fill time calculated from the image processing to the known fill times. The known fill times are the ones calculated with the assigned set of permeability. The average relative error between the calculated fill time from the fitting of the ellipse and the known fill times was found to be less than 5%. The semi-major and minor diameters, the angle of rotation, and the centroid location of the ellipse are also generated in this step. The centroid location of the ellipse on the top side is found in relation with the one on the bottom side which is the center of injection gate. This information is used to determine the initial set of in plane permeability components (K_{xx}, K_{yy}, and K_{xy}) using the analytical solution for resin flow in 2D. These permeability values are not final for 3D flow, they serve as a good starting point for the six parameter optimization search. The semi-major and minor diameters of the fitted ellipse at different times are input values to calculate in-plane permeability (K_{xx} and K_{yy}). The rotation angle is directly related to the magnitude of in-plane skew term (K_{xy}). The initial in-plane permeability (K_{xx}, K_{yy}, and K_{xy}) are calculated using the Eqs. (4)–(6) [1]:

$$K_{xx} = \frac{\mu \varnothing}{6\Delta p}\left[\frac{2x_f^3}{r_0} - 3x_f^2 + r_0^2\right]\frac{1}{t_{fx}} \tag{4}$$

$$K_{yy} = \frac{\mu \varnothing}{6\Delta p}\left[\frac{2y_f^3}{r_0} - 3y_f^2 + r_0^2\right]\frac{1}{t_{fy}} \tag{5}$$

$$K_{xy} = \frac{1}{2}(K_{yy} - K_{xx})\tan(2\theta) \tag{6}$$

Here, the r_0 is the inlet radius, x_f and y_f are the flow front positions along x and y axis at times t_{fx} and t_{fy}. The Δp is the applied pressure difference driving the simulated resin through a preform, μ is the

viscosity of the impregnating resin, and $\varnothing$ is the preform porosity. θ is the angle which represents the orientation of the flow front ellipse with respect to experimental set-up axis.

The algorithm to find the optimal values needs an initial value for all the six independent components of the permeability tensor. The through thickness permeability components K_{xz}, K_{yz}, and K_{zz}, are obtained through grid search method described in the next section using the same image processing information.

The advantage of this image processing method is that it is easy and simple to use. For example, Okonkwo et al. [1] reported that 192 sensors installed on the top and bottom molds were used to obtain the resin arrival times. The maintenance of sensors is challenging and also makes cleaning of the mold difficult because some of resin gets embedded in the sensors even after cleaning which compromises the accuracy of the measurement. Compared to the method using sensors, image processing requires only two cameras which makes the methodology convenient. However the downside is that one must use molds that have a transparent window.

2.4. Grid search method

The Grid method was introduced because a good estimate of the initial value for through the thickness components (K_{xz}, K_{yz}, and K_{zz}) is crucial to prevent the optimization search with the simplex method to get trapped in a local minima. Finding a global minima without getting trapped in a local minima has been an important issue for simplex algorithms. There have been multiple efforts to improve the *Nelder Meade simplex method*. [13–16]. Chelouah and Siarry [13] proposed a new hybrid method composed of a genetic algorithm and simplex search to resolve the issue in 2012. The hybrid method is called *Continuous Genetic Algorithm* (CGA). In CGA, a promising population is found first using a genetic algorithm. Later, Chelouah and Siarry employed a new hybrid method combining a *Tabu* search and the *Nelder Meade simplex search* to address the issue of local minima. *Tabu* search is described in the journal by Hertz and Werra et al. [17] The combination of the two search methods allowed the localization of the promising region with a global minima [13,14].

In this study, grid method conducted an initial search in the most promising region to provide a global minima and was implemented before the simplex search step to prevent the simplex search from being trapped in a local minima. The initial search using the grid method, is carried out by estimating through thickness skew terms from what is known about the flow along the top and the bottom surface. First, the ratio between K_{xz} and K_{yz} is obtained from the center shift of flow front appearing on the top side compared to the bottom side from the experimental results. The ratio of x-shift and y-shift gives the ratio between K_{xz} and K_{yz} (as is clear from Fig. 1). This reduces 6 variable optimization to 5 variable optimization problem.

$$K_{yz} = K_{xz}R \tag{7}$$

Here, the ratio, R is defined as the distance of the center of the ellipse on the top surface from the injection location along the bottom surface in the x direction to that in y direction as can be seen in Fig. 1.

Initial $K_{zz,ini}$ and $K_{xz,ini}$ are defined as follows

$$K_{zz,ini} = \frac{0.01(K_{xx} + K_{yy})}{2} \tag{8}$$

As the through thickness *Kzz* is usually two order of magnitude smaller than the smallest in plane permeability.

$$K_{xz,ini} = \sqrt{K_{xx}K_{zz}} \tag{9}$$

$K_{xz,ini}$ is calculated using Eq. (9) as it needs to satisfy positive definite condition as permeability cannot be a negative value.

The grid search method takes the initial $K_{zz,ini}$ and $K_{xz,ini}$, values and searches for the optimum initial guess in its neighborhood as shown in Fig. 5. $K_{zz,ini}$ is varied from 0.1 $K_{zz,ini}$ to 1.5 $K_{zz,ini}$ while $K_{xz,ini}$ is varied from 0.1 $K_{xz,ini}$, to $K_{xz,ini}$ to create the input set for LIMS along with the other permeability components defined by Eqs. (4)–(7). The results are compared with the experimental arrival times at the nodes and RSS is calculated for each grid point as shown in Fig. 5.

The set of permeability (K_{zz}, K_{xz}) that yields the lowest RSS value is chosen as the initial guess along with Eqs. (4)–(7) initial values for the simple method. This is a necessary step to ensure successful convergence of simplex search to find a global minima which will provide us with the six independent permeability components that match the experimental flow arrival times along the top and the bottom surfaces at various time steps. We assume here that one unique set of permeability values will provide this global minimum as the flow front motion along the top and the bottom surface has one correspondence with one unique permeability tensor.

2.5. The simplex method

Simplex method can minimize a function of n variables. Simplex is a convex hull with $n + 1$ vertices in n dimensions. The function of

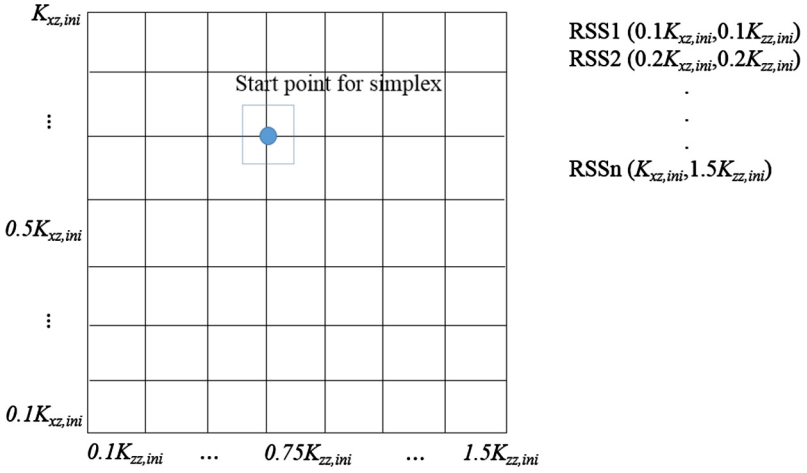

Fig. 5. Grid search method to find the best initial guess for $K_{zz,ini}$ and for $K_{xz,ini}$. $K_{zz,ini}$ is varied from $0.1K_{zz,ini}$ to $1.5K_{zz,ini}$, $K_{xz,ini}$ is varied from $0.1K_{xz,ini}$ to $K_{xz,ini}$. (For interpretation of the references to color in this figure legend, the reader is referred to the web version of this article.)

Table 1
Assigned set of six components of permeability.

	K_{xx} (m^2)	K_{yy} (m^2)	K_{zz} (m^2)	K_{xy} (m^2)	K_{xz} (m^2)	K_{yz} (m^2)
Numerical value:	2e−10	1e−10	1e−12	1e−11	5e−12	5e−12

Table 2
Parameter values for LIMS simulation.

Parameter	Numerical value
Inlet pressure (Pa)	10^5
Volume fraction (%)	40
Viscosity of resin (Pa s)	0.1
Diameter of inlet gate (cm)	3.81

n variables is minimized through a transformation of the simplex convex hull figure through reflection, contraction, and extension. n vertices of the convex hull without an origin vertex decides the vector direction for the transformation. Function values at the (n + 1) vertices of simplex are compared and the vertex with the highest function value is replaced by another point. The process is terminated when the function value is minimized which satisfies the assigned tolerance. It is a very powerful and quick method that can optimize a function of a large number of variables [18]. Okonkwo el al. chose a golden search method for 4 variable optimization [1]. When the golden search method was implemented to optimize a function of 6 variables, the operation time took more than 10 h. The slow convergence is a well-known drawback of a golden search method with more than 3 variables. Simplex can deal with multiple variables in a comparably shorter operation time of a couple of hours.

For the final step in the optimized methodology, the simplex search begins with the initial set of six permeability components as determined from the grid search method as described in the previous section. The simplex algorithm then continues to minimize the RSS of fill times between the experiment and the simulation at various time steps. When the average of relative error of all fill times becomes less than 5%, the simplex search is deemed to be converged and the search is terminated. The entire system is automated in that image processing, grid method, and simplex are all coded and linked together in MATLAB program coupled with LIMS. Once the images are recorded from an experiment, the entire algorithm is carried out automatically and reports the six independent components of the permeability tensor.

3. Results

The presented algorithm is validated through virtual and actual experiments.

3.1. Virtual experiment

The accuracy of the developed algorithm as described in the previous section was evaluated numerically with LIMS simulation data. First, a set of six permeability components was assigned as an input to LIMS to generate the nodal arrival times (nodal fill times data). The assigned permeability set is given in Table 1. The process parameters for simulation are presented in Table 2.

Transverse skew terms (K_{yz} *and* K_{xz}) are assigned with a moderate value to test the search-ability of the algorithm in the presence of skew terms. Visual images of simulated flow fronts from LIMS at different times were captured into image files as if they were recorded experimental images to be used later for image processing. From the image processing data, the found initial set of permeability (K_{xx} 2e−10 m^2, K_{yy} 6e−11 m^2, K_{zz} 1.3e−12 m^2, K_{xy} 8e−12 m^2, K_{xz} 4e−12 m^2, and K_{yz} 1e−12 m^2) is optimized by the simplex search.

The result in Table 3 shows the prediction is within 2% of error. The superimposed flow fronts presented in Fig. 6 shows a good agreement between predicted and numerically calculated flow fronts. One important point to notice in Fig. 6 is the shift of origin in the presence of skew terms as pointed out earlier. The shift of

Table 3
Predicted permeability (m^2) and its relative error (%).

	K_{xx} (m^2)	K_{yy} (m^2)	K_{zz} (m^2)	K_{xy} (m^2)	K_{xz} (m^2)	K_{yz} (m^2)
Predicted Permeability (m^2)	1.97e−10	9.8e−11	9.9e−13	1e−11	5.01e−12	4.98e−12
Relative Error (%)	1.05	1.16	1.05	0.05	1.03	1.06

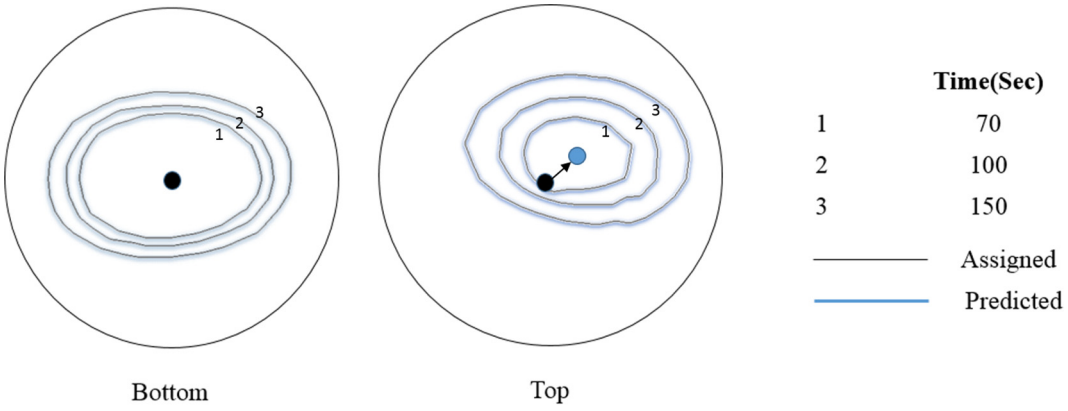

Fig. 6. Predicted flow fronts superimposed on numerically obtained flow fronts along the top and the bottom surface at time of 70, 100,150 s. Black dot represents the inlet gate. (For interpretation of the references to color in this figure legend, the reader is referred to the web version of this article.)

Table 4
Experimental conditions for the permeability characterization test.

Parameter	Numerical value
Inlet pressure (Pa)	110,000
Volume fraction of E-glass (%)	54
Viscosity of corn syrup (Pa s)	0.098
Diameter of inlet gate (cm)	3.81
Dimension of acrylic plate (cm)	30.58 × 30.58

origin occurred both in x and y direction with both skew terms. The algorithm accurately predicted all of the six permeability components and converged in less than two hours of CPU time on a PC computer.

3.2. 3D fabric permeability characterization

3D woven E glass fabric with 6230 g/m^2 aerial density was used as a reinforcement sample. Two layers of the fabric were used and the spacer plate of 4.5 mm was used. Acrylic plastic plate reinforced with steel plate to prevent deformation was used as a mold. Corn syrup was used as a test fluid for convenience. 3D flow experiment was carried out in the setting shown in Fig. 4. Experimental conditions are displayed in Table 4. The proposed methodology was used to characterize the permeability tensor. Initial permeability tensor found (K_{xx} 1.2e−10 m^2, K_{yy} 2.7e−09 m^2, K_{zz} 1.4e−12 m^2, K_{xy}1e−14 m^2, K_{xz} 1e−11 m^2, and K_{yz} 1e−12 m^2) was optimized with Simplex method. The results are presented in Figs. 7 and 8 and Table 5. Fig. 7 shows the experimental flow front, the flow front from numerical simulation with predicted permeability and the comparison at 6 s between the two for both the top and bottom side.

The superimposed images from experiment and numerical simulation are presented in Fig. 8. The experimental result shows a good agreement with predicted flows on both the top and bottom sides. The predicted set of permeability seems reasonable based on the shape of the flow front on the bottom and top surfaces. Firstly, K_{xx} value is about 6 times smaller than K_{yy} value, which can be explained that the ratio of major axis of an ellipse at 6 s in y direction to minor axis in x direction is found to be 2.3. The square of the ratio of major to minor axis of ellipse gives a good approximation of K_{yy} to K_{xx} ratio. The square of the ratio is about 5.5 which shows a good approximation for the ratio of predicted in plane permeability ratio of 6.25. As the measured rotation angle of the ellipse is 0.6° on average with respect to the coordinate direction, we would expect K_{xy} to be very insignificant. The result shows that K_{xy} is four orders of magnitude smaller than other in plane permeability component confirming what is observed that the principal directions of the fabrics are very much aligned with the coordinate direction in the x-y in plane direction. K_{yz} and K_{xz} causes a shift of the center of

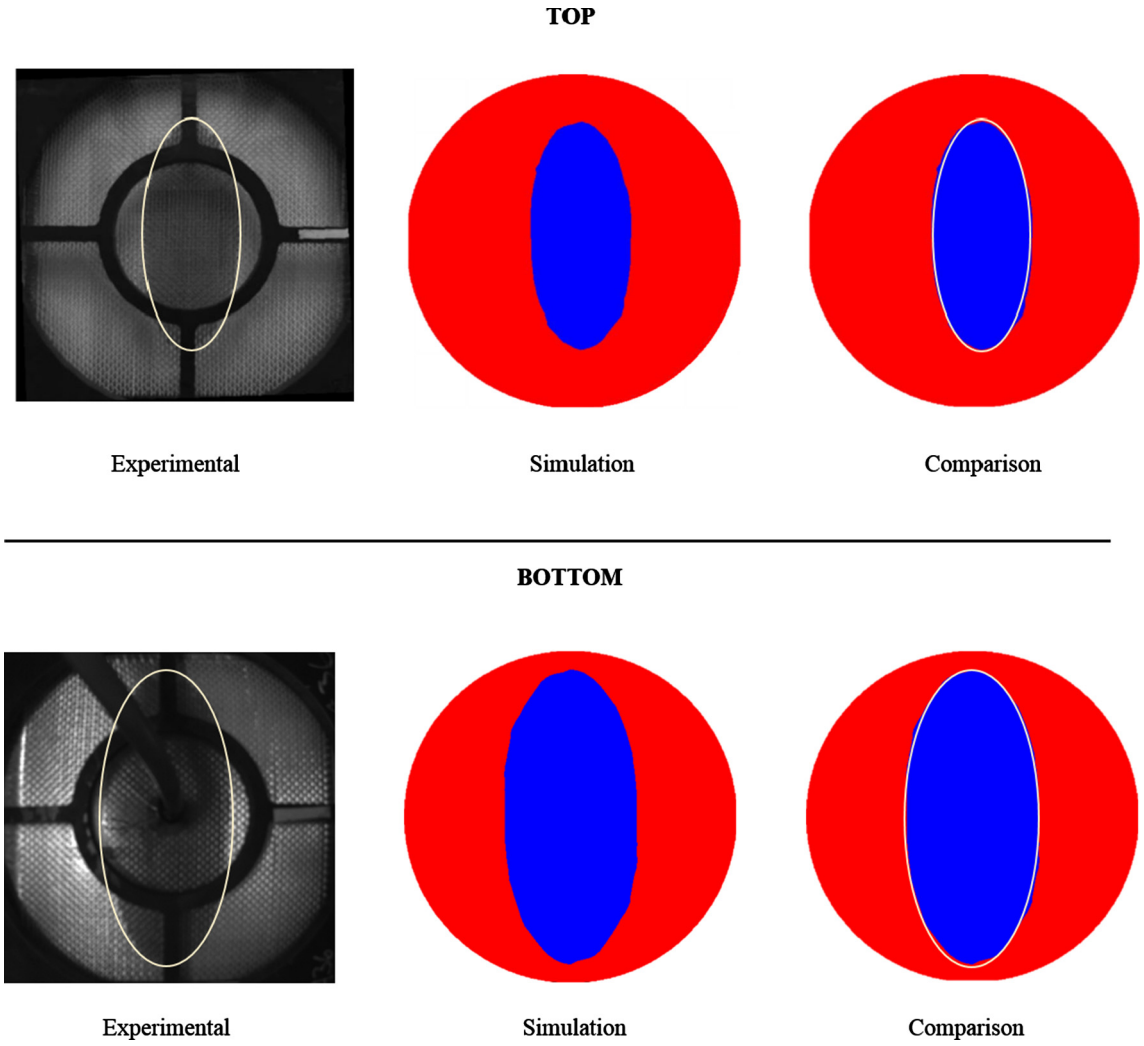

Fig. 7. Experimental flow front, the flow front from numerical simulation with predicted permeability and the comparison at 6 s between two for both the top and bottom side. (For interpretation of the references to color in this figure legend, the reader is referred to the web version of this article.)

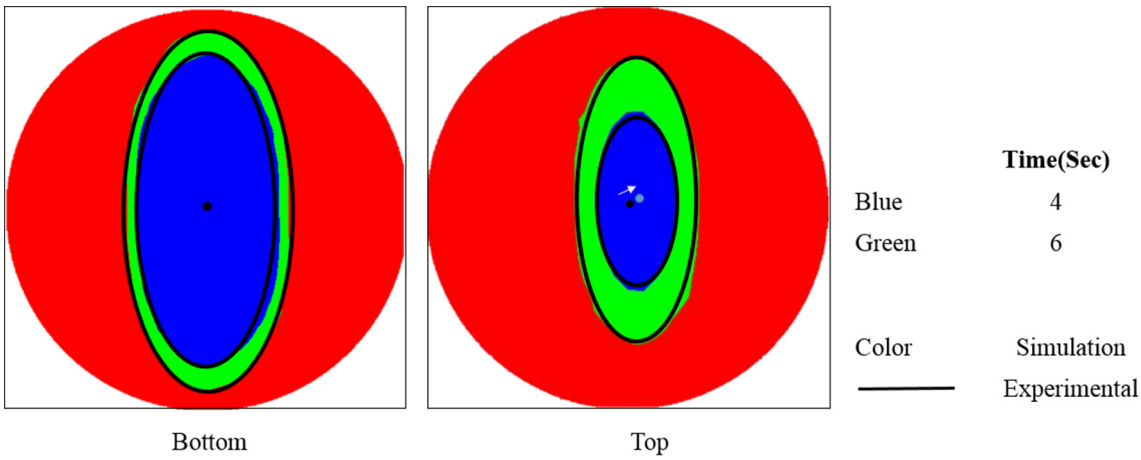

Fig. 8. Predicted flow front superimposed on experimental flow front on the top and bottom at different times. (For interpretation of the references to color in this figure legend, the reader is referred to the web version of this article.)

Table 5
Predicted six components of permeability tensor of 3D glass fabric.

	K_{xx} (m^2)	K_{yy} (m^2)	K_{zz} (m^2)	K_{xy} (m^2)	K_{xz} (m^2)	K_{yz} (m^2)
Numerical value:	3.2e−10	2e−09	4e−12	6.7e−14	7e−12	4.5e−12

the ellipse on the top side. The measured center shift of ellipse on the top is 8.5 mm in the x direction and 6.5 mm in the y direction. The shifts of the center of the top side ellipse in both directions explains the significant skew terms which are of the same order as K_{zz}. 1D and 2D flow experiments were carried out with the same 3D glass fabric. K_{zz} was found to be 4.7e−12 m^2 from the 1D flow test. K_{xx} and K_{yy} were found from 2D radial flow experiment. K_{xx} is calculated to be 2.04e−10 m^2 and K_{yy} is 2.28e−09 m^2. The degree of rotation of the ellipse from 2D experiment was measured to be less than 1 degree, which agrees with the negligible magnitude of K_{xy} measured from 3D flow. The measured permeability from 1D and 2D experiments agree with the set of permeability found from 3D permeability well within the range of 20–30%.

4. Summary and conclusions

An optimized algorithm has been developed to find all of the six independent components of the permeability tensor of a fiber preform from a single experiment. A 3D radial flow experiment was developed to record the movement of the flow front along the top and the bottom surface. With image processing algorithms information about the flow arrival times at various locations and the shape of the ellipses along the top and bottom could be extracted automatically. Initial values of the six independent components of the permeability tensor were successfully found with analytical 2D solution, image information captured via recording the movement of the flow front through transparent mold walls along the top and the bottom surface, and the grid search method. The simulation resin flow arrival times were compared with the experimental values at all time steps with the goal of minimizing the error. The grid search method allowed the simplex search to reach a global minima without getting trapped in a local minima. Simplex method was found to be highly advantageous with more than 3 variables over other search methods such as golden search method. Thus our methodology provide the six components of the 3D permeability tensor from a single experiment due to its unique relationship with the flow front arrival data at various locations along the top and the bottom surface of the mold. The best validation of the method is to see when you prescribe certain permeability tensor in a flow simulation and then take the arrival times of the flow at selected location in the simulation and use our methodology – can we recover the assigned permeability? We have shown this conclusively in one of the example which validates the method. The proposed methodology showed an accurate and fast convergence which matched the simulation flow fronts with the experimental ones. The result of the experimental study shows that the permeability set of 3D fabric can possess the skew terms which causes resin to flow in skewed way in through the thickness direction as was shown in Fig. 2. Hence, it is essential to identify all six components of permeability set to fully understand resin flow through unbalanced and 3D fabrics during LCM process. The automated permeability work station is easy to use and can determine all six independent components of the 3D fabric permeability tensor from a single experiment.

Acknowledgement

We would like to thank Steve Davis for his help with the experimental set-up. Also, the authors thankfully acknowledge Tess Carella and Louis Agostino for their help with experiments.

References

[1] Okonkwo K, Simacek P, Advani SG, Parnas RS. Characterization of 3D fiber preform permeability tensor in radial flow using an inverse algorithm based on sensors and simulation. Compos Part A Appl Sci Manuf 2011;42(10):1283–92.
[2] Cai Z. Estimation of the permeability of fibrous preforms for resin transfer moulding processes. Compos Manuf 1992;3(4):251–7.
[3] Demaría FTC, Ruiz Edu. In-plane anisotropic permeability characterization of deformed woven fabrics by unidirectional injection. Part I: Experimental results. Polym Polym Compos 2008;16(2):101–13.
[4] Vernet N, Ruiz E, Advani S, Alms JB, Aubert M, Barburski M, et al. Experimental determination of the permeability of engineering textiles: benchmark II. Compos Part A Appl Sci Manuf 2014;61:172–84.
[5] Arbter R, Beraud JM, Binetruy C, Bizet L, Breard J, Comas-Cardona S, et al. Experimental determination of the permeability of textiles: a benchmark exercise. Compos Part A Appl Sci Manuf 2011;42(9):1157–68.
[6] Sharma S, Siginer DA. Permeability measurement methods in porous media of fiber reinforced composites. Appl Mech Rev 2010;63(2):020802.

[7] Weitzenbock JR, Shenoi RA, Wilson PA. Radial flow permeability measurement. Part A: Theory. Compos Part A Appl Sci Manuf 1999;30(6):781–96.
[8] Lawrence JM, Barr J, Karmakar R, Advani SG. Characterization of preform permeability in the presence of race tracking. Compos Part A Appl Sci Manuf 2004;35(12):1393–405.
[9] Nedanov P, Advani SG. A method to determine 3D permeability of fibrous reinforcements. J Compos Mater 2002;36(02):241–54.
[10] Woerdeman DL, Phelan FR, Parnas RS. Interpretation of 3-D permeability measurements for RTM modeling. Polym Compos 1995;16(6):7–12.
[11] Hatice Sas SGA, Simacek Pavel, Yun Minyoung, Agostino Louis. A new approach for textile fiber preform permeability tensor characterization with non-zero skew components. In: Texcomp -12 conf.. p. 26–9.
[12] Han KK, Lee CW, Rice BP. Measurements of the permeability of fiber preforms and applications. Compos Sci Technol 2000;60(12–13):2435–41.
[13] Chelouah R, Siarry P. A hybrid method combining continuous tabu search and Nelder-Mead simplex algorithms for the global optimization of multiminima functions. Eur J Oper Res 2005;161(3):636–54.
[14] Chelouah R, Siarry P. Genetic and Nelder-Mead algorithms hybridized for a more accurate global optimization of continuous multiminima functions. Eur J Oper Res 2003;148(2):335–48.
[15] Fan SKS, Liang YC, Zahara E. A genetic algorithm and a particle swarm optimizer hybridized with Nelder-Mead simplex search. Comput Ind Eng 2006;50(4):401–25.
[16] Fan SKS, Zahara E. A hybrid simplex search and particle swarm optimization for unconstrained optimization. Eur J Oper Res 2007;181(2):527–48.
[17] Hertz A, Werra D. Using tabu search techniques for graph coloring. Computing 1987;39(4):345–51.
[18] Nelder Ja, Mead R. A simplex method for function minimization. Comput J 1964;7(4):308–13.